


Building ground states of the Hubbard model by time-ordered bound-pair injectionK. L. Zhang  and Z. Song **School of Physics, Nankai University, Tianjin 300071, China* (Received 17 August 2021; revised 29 October 2021; accepted 16 December 2021; published 28 December 2021)

According to energy band theory, ground states of a normal conductor and insulator can be obtained by filling electrons individually into energy levels, without any restrictions. It fails when the electron-electron correlation is taken into account. In this work, we investigate the dynamic process of building ground states of a Hubbard model. It is based on time-ordered quantum quenches for unidirectional hopping across a central and an auxiliary Hubbard model. We find that there exists a set of optimal parameters (chemical potentials and pair binding energy) for the auxiliary system, which takes the role of electron-pair reservoir. The exceptional point dynamics in non-Hermitian quantum mechanics allows the perfect transfer of electron pair from the reservoir to the central system, obtaining its ground states at different fillings. The dynamics of time-ordered pair filling not only provides a method for correlated quantum state engineering, but also reveals the feature of the ground state in an alternative way.

DOI: [10.1103/PhysRevB.104.245140](https://doi.org/10.1103/PhysRevB.104.245140)**I. INTRODUCTION**

Understanding the quantum states of strongly interacting many-body systems via quantum dynamics is one of the promising methods in contemporary condensed matter physics. Compared to weakly or noninteracting systems, strong interactions can induce fascinating phenomena, which cannot be understood by conventional band theory. One example is the Mott insulating state: for the ground state of a fermionic lattice system with a half-filled band, strong interactions can make this system insulating [1–3] from the conducting state. The essence of what happens is correlation between two fermions with opposite spins. High-temperature superconductivity, as another example, can arise from the correlated motion of holes in an antiferromagnetic Mott insulator [4,5]. Theoretically, such a correlation can be characterized by the correlation function. However, it is a challenge to measure the correlation function in the experiment [6]. Recently, correlated insulator has attracted much attention due to the discovery of twisted bilayer graphene [7–13].

A conceptually clear and frequently used dynamic approach is a quantum quench, where one starts in the ground state of a given Hamiltonian and then suddenly changes the parameters of this Hamiltonian. After a sufficiently long time, the evolved state may deviate from the ground state and is not the eigenstate of the quenched Hamiltonian in general, since the process is nonadiabatic. Nevertheless, it is expected that the nonequilibrium state contains both the information of initial and final Hamiltonians. Many research efforts have been devoted to this subject [14–26].

In normal conductors and insulators, the situation is well described by free electron theory, where the electrons behave as free particles. Viewed in this context, electrons can be

injected into or emitted from the material individually. Technically, the ground state of free electron gas can be built by a dynamic process in the framework of quantum mechanics. A natural question is how, in the presence of interaction between electrons with opposite spins, a correlated many-body ground state is formed dynamically. Despite being a great computational challenge for simulating the dynamics in large size quantum many-body systems, theoretical calculations on small sized systems may provide new insights into the experimental observations. Recent advances in quantum simulations of the Hubbard model with ultracold atoms have offer a multifunctional platform to unveil properties of the strongly correlated system [6,27–38].

In this work, we propose a method to build ground states of a Hubbard model in the framework of quantum dynamics. It is an extension of the conventional quenching method, switching a system from N -site to $(N + 1)$ -site lattices. We focus on an N -site Hubbard model with a side-coupled site. Initially, the central system is set in ground state at a certain filling and the side-coupled site is empty. We consider two types of side-coupling strength—Hermitian and non-Hermitian [39–44] ones. In the Hermitian case, analytical analysis and numerical simulation show that there exist optimal parameters, chemical potential and pair binding energy, for the extra site, with which the time evolution exhibits perfect oscillation, indicating that a bound pair of electrons can be extracted and returned back to the central system coherently. In the non-Hermitian case with unidirectional hopping, the exceptional point (EP) [42–44] dynamics allows the complete transfer of electron pair between the central system and the extra site. Furthermore, we investigate the dynamic process of building ground states of a Hubbard model. It bases on time-ordered quantum quenches for unidirectional hopping across a central and an auxiliary Hubbard model. Finally, we provide a scanning scheme to determine the quenching parameters. Numerical simulation for small-size one-dimensional (1D) and two-dimensional (2D)

*songtc@nankai.edu.cn

systems shows that the ground states at different fillings can be built coherently with high fidelity. Our finding not only provides a method for correlated quantum state engineering, but also reveals the feature of the ground state in an alternative way.

This paper is organized as follows. In Sec. II, we introduce the model Hamiltonian and study the dynamics of single-pair oscillation. In Sec. III, we investigate the dynamics of complete pair transport by a non-Hermitian method. In Sec. IV, we propose a dynamical way to build the ground state of the Hubbard model by time-ordered bound-pair injection. In Sec. V, we provide a scanning scheme to determine the quenching parameters. Finally, we summarize our results in Sec. VI.

II. MODEL AND SINGLE-PAIR OSCILLATION

We consider the Hubbard model H_c connected with a side-coupled site p. The Hamiltonian

$$H = H_c + H_p \quad (1)$$

consists of two parts. Here H_c is a simple Hubbard model on an N -site bipartite lattice with equal sites of two sublattices,

$$H_c = \sum_{l>l'} \sum_{\sigma=\uparrow,\downarrow} (J_{l,l'} c_{l,\sigma}^\dagger c_{l',\sigma} + \text{H.c.}) + \sum_l U_l n_{l,\uparrow} n_{l,\downarrow}, \quad (2)$$

where the operator $c_{l,\sigma}$ ($c_{l,\sigma}^\dagger$) is the usual annihilation (creation) operator of an electron with spin $\sigma \in \{\uparrow, \downarrow\}$ at site l , and $n_{l,\sigma} = c_{l,\sigma}^\dagger c_{l,\sigma}$ is the number operator for a particle of spin σ on site l . The hopping $J_{l,l'}$ and interaction U_l are required to be real; the system can be divided into two sublattices A and B such that $J_{l,l'} = 0$ whenever $l, l' \in \{A\}$ or $l, l' \in \{B\}$, and the dimension of the lattice is not yet assumed. The side-coupled term is

$$H_p = J_p \sum_{\sigma=\uparrow,\downarrow} c_{\alpha,\sigma}^\dagger c_{p,\sigma} + \text{H.c.} \\ + U_b n_{p,\uparrow} n_{p,\downarrow} + \mu_\uparrow n_{p,\uparrow} + \mu_\downarrow n_{p,\downarrow}, \quad (3)$$

where $c_{p,\sigma}$ is the annihilation operator of an electron with spin σ on the side-coupled site p; $\alpha \in \{A, B\}$; μ_σ is the chemical potential of the electron with spin σ and U_b is the binding energy of electron pair on the p site. In this work, we mainly consider the case with N -electron filling.

We first review some well-known model properties of the Hubbard model H_c that are crucial to our conclusion. At first, H_c possesses SU(2) symmetry

$$[s^\pm, H_c] = [s^z, H_c] = 0, \quad (4)$$

with $s^+ = (s^-)^\dagger = \sum_l s_l^+$ and $s^z = \sum_l s_l^z$, where the local operators $s_l^+ = c_{l,\uparrow}^\dagger c_{l,\downarrow}$ and $s_l^z = (n_{l,\uparrow} - n_{l,\downarrow})/2$ obey the Lie algebra, that is

$$[s_l^+, s_l^-] = 2s_l^z, [s_l^z, s_l^\pm] = \pm s_l^\pm. \quad (5)$$

Secondly, H_c has spin reversal symmetry defined by

$$\mathcal{T} H_c \mathcal{T}^{-1} = H_c, \quad (6)$$

where \mathcal{T} is the spin reversal operator with the action $\mathcal{T} c_{l,\uparrow} \mathcal{T}^{-1} = c_{l,\downarrow}$ and $\mathcal{T} c_{l,\downarrow} \mathcal{T}^{-1} = c_{l,\uparrow}$ for all l . Then the eigenstates of H_c are also the eigenstates of operators s and s^z . And any eigenstates with nonzero s must be degenerate.

In addition, according to Lieb's theorem [45] for a bipartite lattice, in the repulsive case $U_l = U > 0$, the ground state of H_c at half filling is unique and has spin $s = 0$. The following considerations are based on these properties.

We are interested in the lowest energy eigenstates of H_c in the invariant subspaces with the numbers of electrons n ($s^z = 0$), $n - 1$ ($s^z = \pm 1/2$), and $n - 2$ ($s^z = 0$), respectively. Here n is set to an even number satisfying $2 \leq n \leq N$. The corresponding Schrödinger equations are

$$[H_c - E_g(n, 0)] |\psi_g(n, 0)\rangle = 0, \\ [H_c - E_g(n - 1, \pm 1/2)] |\psi_g(n - 1, \pm 1/2)\rangle = 0, \\ [H_c - E_g(n - 2, 0)] |\psi_g(n - 2, 0)\rangle = 0, \quad (7)$$

where E_g is the ground-state energy in each invariant subspace and $E_g(n - 1, 1/2) = E_g(n - 1, -1/2)$ according to symmetries in the above analysis.

Now we consider the system with H in the subspace spanned by the basis set

$$|1\rangle = |\psi_g(n, 0)\rangle |0\rangle_p, \\ |2\rangle = |\psi_g(n - 1, -1/2)\rangle |\uparrow\rangle_p, \\ |3\rangle = |\psi_g(n - 1, 1/2)\rangle |\downarrow\rangle_p, \\ |4\rangle = |\psi_g(n - 2, 0)\rangle |\uparrow\downarrow\rangle_p, \quad (8)$$

where $|0\rangle_p$ is the vacuum state of the side-coupled site and $|\sigma\rangle_p = c_{p,\sigma}^\dagger |0\rangle_p$, $|\uparrow\downarrow\rangle_p = c_{p,\uparrow}^\dagger c_{p,\downarrow}^\dagger |0\rangle_p$. Based on the basis set, the matrix representation of the effective Hamiltonian for system H is

$$h = \begin{pmatrix} \epsilon_1 & \kappa_1 & \kappa_1 & 0 \\ \kappa_1 & \epsilon_2 & 0 & \kappa_2 \\ \kappa_1 & 0 & \epsilon_3 & \kappa_2 \\ 0 & \kappa_2 & \kappa_2 & \epsilon_4 \end{pmatrix}, \quad (9)$$

where the matrix elements

$$\epsilon_1 = E_g(n, 0), \quad \epsilon_2 = E_g(n - 1, 1/2) + \mu_\uparrow, \\ \epsilon_3 = E_g(n - 1, 1/2) + \mu_\downarrow, \\ \epsilon_4 = E_g(n - 2, 0) + \mu_\uparrow + \mu_\downarrow + U_b, \\ \kappa_1 = \langle 1|H_p|2\rangle = \langle 1|H_p|3\rangle = \langle 2|H_p|1\rangle = \langle 3|H_p|1\rangle, \\ \kappa_2 = \langle 2|H_p|4\rangle = \langle 3|H_p|4\rangle = \langle 4|H_p|2\rangle = \langle 4|H_p|3\rangle. \quad (10)$$

In this framework, parameters $\{\mu_\uparrow, \mu_\downarrow, U_b\}$ determine the dynamics of electron transport. We consider the following three situations.

(i) $|\mu_\downarrow| \gg \mu_\uparrow = E_g(n, 0) - E_g(n - 1, 1/2)$; matrix h reduces to

$$h_\uparrow = \kappa_1 (|1\rangle\langle 2| + |2\rangle\langle 1|) + \epsilon_1 (|1\rangle\langle 1| + |2\rangle\langle 2|). \quad (11)$$

(ii) $|\mu_\uparrow| \gg \mu_\downarrow = E_g(n, 0) - E_g(n - 1, 1/2)$; matrix h reduces to

$$h_\downarrow = \kappa_1 (|1\rangle\langle 3| + |3\rangle\langle 1|) + \epsilon_1 (|1\rangle\langle 1| + |3\rangle\langle 3|). \quad (12)$$

In these two cases, one of the polarized electrons is excluded at the p site. The dynamics is single-electron oscillation, realizing perfect transport from the center system to the p site. We are interested in the third case, where spin-up and spin-down electrons are all in resonance.

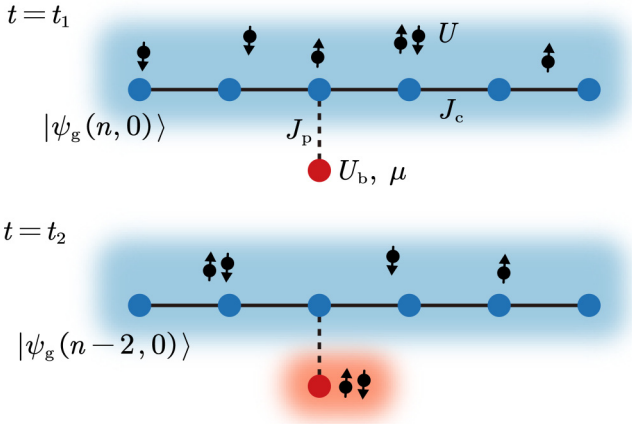


FIG. 1. Schematic of the complete pair resonance in the Hubbard chain. At instant $t = t_1$, the center system (blue region) is prepared in n -particle ground state and the side-coupled site (red dot) is empty. With certain pair binding energy U_b and chemical potential μ [Eq. (13)] of the side-coupled site, an electron pair is resonantly transmitted to the side-coupled site, and the center system remains in the $(n - 2)$ -particle ground state at instant $t = t_2$.

(iii) When taking the parameters as

$$\begin{aligned} \mu_\uparrow = \mu_\downarrow = \mu &= E_g(n, 0) - E_g(n - 1, 1/2), \\ U_b &= 2E_g(n - 1, 1/2) - E_g(n - 2, 0) - E_g(n, 0), \end{aligned} \quad (13)$$

matrix h reduces to

$$h_R = \begin{pmatrix} 0 & \kappa_1 & \kappa_1 & 0 \\ \kappa_1 & 0 & 0 & \kappa_2 \\ \kappa_1 & 0 & 0 & \kappa_2 \\ 0 & \kappa_2 & \kappa_2 & 0 \end{pmatrix} + E_g(n, 0). \quad (14)$$

It supports periodic dynamics with period $T = 2\pi/\varepsilon$ [$\varepsilon = \sqrt{2(\kappa_1^2 + \kappa_2^2)}$], since the energy levels are always equally spaced ε , and importantly allows the time evolution

$$\begin{aligned} |\psi(t)\rangle &= e^{-ih_R t} |1\rangle = \frac{1}{2(\kappa_1^2 + \kappa_2^2)} \\ &\times \{ [2\kappa_1^2 \cos(\varepsilon t) + 2\kappa_2^2] |1\rangle - i\varepsilon\kappa_1 \sin(\varepsilon t) (|2\rangle + |3\rangle) \\ &+ [2\kappa_2\kappa_1 \cos(\varepsilon t) - 2\kappa_2\kappa_1] |4\rangle \} \end{aligned} \quad (15)$$

for the initial state $|\psi_g(N, 0)\rangle|0\rangle_p$. It demonstrates a pair oscillation between the center system and the side-coupled site, indicating that a pair of electrons can be extracted from the ground state of H_c at instant $(m + 1/2)T$ ($m = 0, 1, 2, 3, \dots$) in the small J_p limit. The maximal pair transport is

$$\max[|4|\psi(t)\rangle|^2] = \frac{4(\kappa_2\kappa_1)^2}{(\kappa_1^2 + \kappa_2^2)^2}, \quad (16)$$

which turns to unit at $\kappa_1 = \kappa_2$, indicating complete pair transport. The schematic illustration of this process for a 1D system is shown in Fig. 1, although the above analysis is not limited to 1D.

For zero U , the ground states of H_c in each invariant subspace have simple relations

$$\begin{aligned} |\psi_g(n, 0)\rangle &= c_{F,\uparrow}^\dagger |\psi_g(n - 1, -1/2)\rangle \\ &= -c_{F,\downarrow}^\dagger |\psi_g(n - 1, 1/2)\rangle \end{aligned} \quad (17)$$

and

$$\begin{aligned} |\psi_g(n - 1, 1/2)\rangle &= c_{F,\uparrow}^\dagger |\psi_g(n - 2, 0)\rangle, \\ |\psi_g(n - 1, -1/2)\rangle &= c_{F,\downarrow}^\dagger |\psi_g(n - 2, 0)\rangle, \end{aligned} \quad (18)$$

where $c_{F,\sigma}^\dagger$ is the creation operator of an electron at Fermi level ε_F . Accordingly, we have

$$\begin{aligned} E_g(n, 0) &= \varepsilon_F + E_g(n - 1, \pm 1/2) \\ &= 2\varepsilon_F + E_g(n - 2, 0). \end{aligned} \quad (19)$$

Obviously, we have $\kappa_1 = \kappa_2$ and $U_b = 0$, which results in complete extraction. This can be understood from the following facts: when $U = 0$, all the dynamics of H in each invariant subspace with fixed electron number is governed by its matrix representation in a single-particle subspace. In the single-particle subspace, H_c can be written as a diagonal form,

$$H_0 = \sum_j \varepsilon_j (|j, \uparrow\rangle\langle j, \uparrow| + |j, \downarrow\rangle\langle j, \downarrow|), \quad (20)$$

where the single-particle eigenstate with eigenenergy ε_j is defined as $|j, \sigma\rangle = A_{j,\sigma}^\dagger |\text{vac}\rangle$ ($\sigma = \uparrow, \downarrow$) and $|\text{vac}\rangle$ is the vacuum state of the electron operator, i.e., $c_{l,\sigma} |\text{vac}\rangle = 0$. For any pair eigenstate

$$|\psi(n, 0)\rangle = \prod_{\{j\}} A_{j,\uparrow}^\dagger A_{j,\downarrow}^\dagger |\text{vac}\rangle, \quad (21)$$

with eigenenergy

$$E(n, 0) = 2 \sum_{\{j\}} \varepsilon_j, \quad (22)$$

where $\{j\}$ is an arbitrary set of energy level indices. We simply have

$$\begin{aligned} |\psi(n - 1, -1/2)\rangle &= A_{j_0,\uparrow} |\psi(n, 0)\rangle, \\ |\psi(n - 1, 1/2)\rangle &= A_{j_0,\downarrow} |\psi(n, 0)\rangle \end{aligned} \quad (23)$$

and

$$\begin{aligned} |\psi(n - 2, 0)\rangle &= A_{j_0,\uparrow} |\psi(n - 1, 1/2)\rangle, \\ &= -A_{j_0,\downarrow} |\psi(n - 1, -1/2)\rangle, \end{aligned} \quad (24)$$

for arbitrary $j_0 \in \{j\}$. Accordingly, we have

$$\begin{aligned} E(n - 1, \pm 1/2) &= 2 \sum_{\{j\}} \varepsilon_j - \varepsilon_{j_0}, \\ E(n - 2, 0) &= 2 \sum_{\{j\}} \varepsilon_j - 2\varepsilon_{j_0}. \end{aligned} \quad (25)$$

Then taking $\mu_\uparrow = \mu_\downarrow = \mu = \varepsilon_{j_0}$ the resonant subspace can be constructed with $\kappa_1 = \kappa_2$ and $U_b = 0$. We conclude that complete pair transport can occur for an arbitrary pair in the zero U system.

For nonzero U , in general, we have $\kappa_1 \neq \kappa_2$, which results in incomplete extraction. However, it is presumably that we

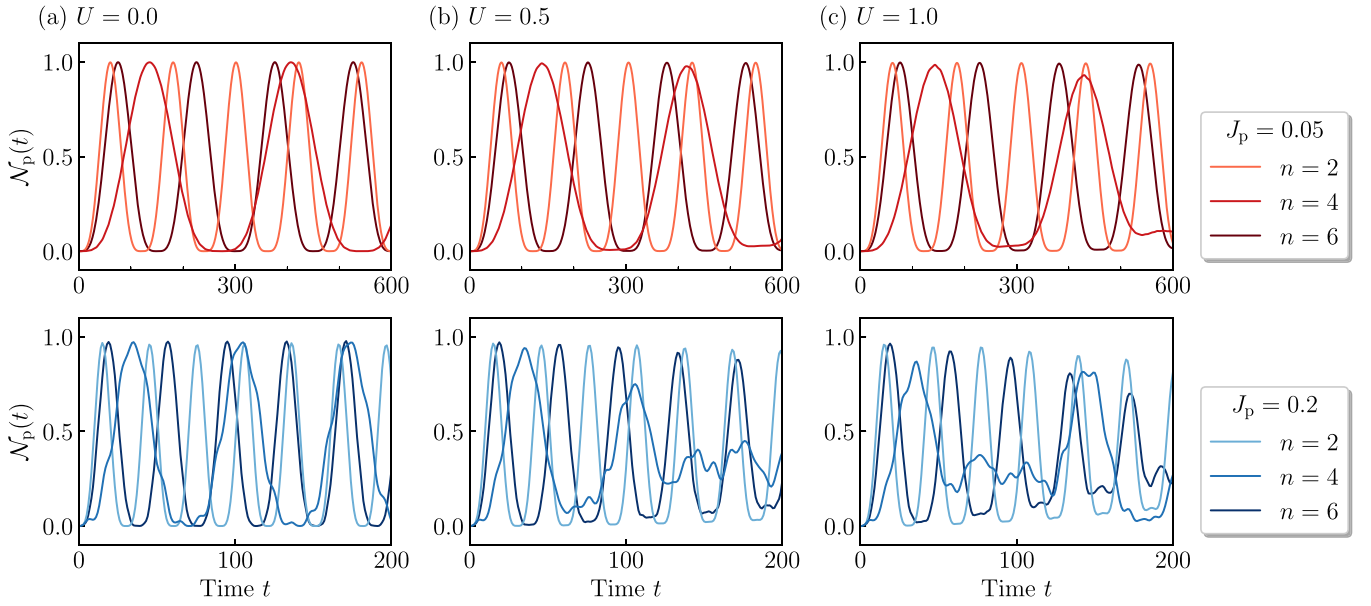


FIG. 2. Numerical results of the electron pair oscillation for different fillings n and values of $U_l = U$: (a) $U = 0$, (b) $U = 0.5$, and (c) $U = 1.0$. The top and bottom panels show the number of electron pairs of the side-coupled site as a function of time t for coupling strength $J_p = 0.05$ and 0.2 , respectively. Initially, the center system with Hubbard interaction U is prepared in the n -particle ground state $|\psi_g(n, 0)\rangle$ of Hamiltonian H_c and the side-coupled site is empty. The pair binding energy U_b and chemical potential μ of the side-coupled site are set to the values defined in Eq. (13), wherein the ground-state energies are obtained by the exact diagonalization of the Hamiltonian H_c in n -, $(n-1)$ -, and $(n-2)$ -particle subspaces. The uniform nearest neighbor hopping is $J_c = 1$ and the system size is $N = 6$.

have $\kappa_1 \approx \kappa_2$ for small U . To verify the above analysis, numerical simulations for a finite 1D system with different fillings n and values of $U_l = U$ are performed. The lattice is illustrated in Fig. 1. The initial state is prepared as $|\psi(t=0)\rangle = |\psi_g(n, 0)\rangle|0\rangle_p$, and the evolved state is calculated as $|\psi(t)\rangle = e^{-iHt}|\psi_g(n, 0)\rangle|0\rangle_p / |e^{-iHt}|\psi_g(n, 0)\rangle|0\rangle_p|$. Here the numerical computations are performed by using a uniform mesh in conducting time discretization. In Fig. 2, we show the number of electron pairs of the side-coupled site as a function of time, which is defined as

$$\mathcal{N}_p(t) = \langle \psi(t) | n_{p,\uparrow} n_{p,\downarrow} | \psi(t) \rangle. \quad (26)$$

We can see that, for small J_p , the electron pair oscillates between the Hubbard chain and the side-coupled site completely. When J_p and U get large, the dynamics of electron pair oscillation become imperfect. It follows that two ground states $|\psi_g(n, 0)\rangle$ and $|\psi_g(n-2, 0)\rangle$ are connected by a pair of electrons with binding energy U_b . It has the implication that a correlated ground state can emit or absorb a bound pair of electrons coherently.

III. COMPLETE PAIR TRANSPORT

In the above section, we have shown that a single electron can be extracted completely from the ground state of a Hubbard model, while partially for a pair of electrons. A natural question is whether one can realize a complete pair extraction via another setup. We reconsider this issue by a non-Hermitian tunneling between H_c and the side-coupled site. The new version of the Hamiltonian is in the form

$$\mathcal{H} = H_c + \mathcal{H}_p, \quad (27)$$

where the non-Hermitian side-coupled term is

$$\mathcal{H}_p = H_p - J_p \sum_{\sigma=\uparrow,\downarrow} c_{\alpha,\sigma}^\dagger c_{p,\sigma} \quad (28)$$

representing unidirectional tunneling. Under the resonant condition, the corresponding matrix representation becomes

$$\tilde{h}_R = \begin{pmatrix} 0 & 0 & 0 & 0 \\ \kappa_1 & 0 & 0 & 0 \\ \kappa_1 & 0 & 0 & 0 \\ 0 & \kappa_2 & \kappa_2 & 0 \end{pmatrix} + E_g(n, 0). \quad (29)$$

Its Jordan form contains a Jordan block of order three and the coalescing state is $|4\rangle = |\psi_g(n-2, 0)\rangle|\uparrow\downarrow\rangle_p$. The EP dynamics allows a particular time evolution of the initial state $|\psi_g(n, 0)\rangle|0\rangle_p$, that is

$$|\psi(t)\rangle = e^{-i\tilde{h}_R t} |1\rangle = |1\rangle - i\kappa_1 t(|2\rangle + |3\rangle) - t^2 \kappa_1 \kappa_2 |4\rangle, \quad (30)$$

which results in a steady final state $|\psi_g(n-2, 0)\rangle|\uparrow\downarrow\rangle_p$ at a time $t|\kappa_1 \kappa_2| \gg |\kappa_1|$. Importantly, unlike the Hermitian system, the result of complete pair extraction is not sensitive to the relation between κ_1 and κ_2 .

In Fig. 3, we shown the numerical results of this process for a finite system with different fillings n and values of U . To facilitate comparison, the parameters of the system and the initial state are the same as that in Fig. 2, except that the coupling between the center system and the side-coupled site is taken as unidirectional. We can see that, for a larger J_p , the evolved state reaches the steady state faster, which is an advantage in comparison to the Hermitian case in Fig. 2.

Intuitively, the result seems to be straightforward due to the unidirectional hopping term in \mathcal{H}_p . We would like to point out that the resonant condition is necessary for the complete

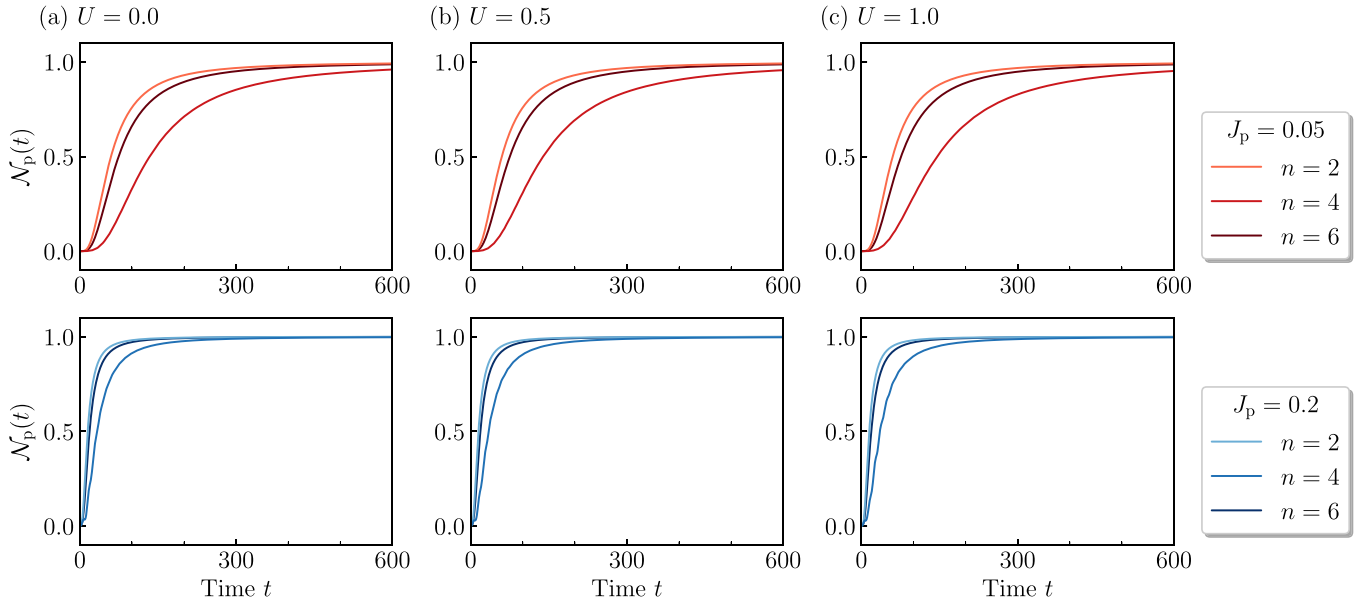


FIG. 3. Numerical results of the complete pair transport for different fillings n and values of U : (a) $U = 0$, (b) $U = 0.5$, and (c) $U = 1.0$. The top and bottom panels show the number of electron pairs of the side-coupled site as a function of time t for unidirectional coupling strength $J_p = 0.05$ and 0.2 , respectively. The parameters of the system and the initial state are the same as that in Fig. 2, except that the coupling between the center system and the side-coupled site is taken as unidirectional.

extraction. A simple derivation can show that any deviation from the resonant condition will result in periodic evolution rather than a steady final state.

IV. TIME-ORDERED BOUND-PAIR INJECTION

In this section, we focus on the possibility to build a ground state of the Hubbard model from an empty system by multipair injections. We consider a Hubbard system with multi-side-coupled sites, which is schematically illustrated in Fig. 4(c). The setup consists of two parts: N -site Hubbard model as a central system and $N/2$ -site decoupled Hubbard model as a reservoir system. The Hamiltonian reads

$$H_1 = H_c + H_r + H_q. \quad (31)$$

Here H_c is taken as the Hubbard chain with uniform hopping $J_{l,l+1} = J_c$ and interaction $U_l = U$; H_r is the reservoir term

$$H_r = \sum_{l=1}^{N/2} [\mu_{2l}(d_{2l,\uparrow}^\dagger d_{2l,\uparrow} + d_{2l,\downarrow}^\dagger d_{2l,\downarrow}) + U_{2l} d_{2l,\uparrow}^\dagger d_{2l,\uparrow} d_{2l,\downarrow}^\dagger d_{2l,\downarrow}] \quad (32)$$

and the quenched term is

$$H_q = \sum_{l=1}^{N/2} \sum_{\sigma=\uparrow,\downarrow} J_{2l}(t) c_{2l,\sigma}^\dagger d_{2l,\sigma}, \quad (33)$$

where $c_{l,\sigma}$ and $d_{l,\sigma}$ are fermion operators and $J_{2l}(t)$ is time dependent. Here both H_c and H_r are Hermitian, describing the central system and reservoir system, respectively. Notably, H_q is a non-Hermitian term, representing the connection between two systems H_c and H_r . The set of parameters $\{\mu_{2l}, U_{2l}\}$ ($l \in [1, N/2]$) are determined by

$$\begin{aligned} \mu_{2l} &= E_g(2l, 0) - E_g(2l - 1, 1/2), \\ U_{2l} &= 2E_g(2l - 1, 1/2) - E_g(2l - 2, 0) - E_g(2l, 0), \end{aligned} \quad (34)$$

where $E_g(L, s_z)$ is the ground-state energy of H_c in L electron and s_z invariant subspace, i.e., $H_c |\psi_g(L, s_z)\rangle = E_g(L, s_z) |\psi_g(L, s_z)\rangle$. In this work, $J_{2l}(t)$ is taken in step functions of time

$$J_{2l}(t) = \begin{cases} 0, & t \leq (l-1)\tau, \\ J, & t > (l-1)\tau. \end{cases} \quad (35)$$

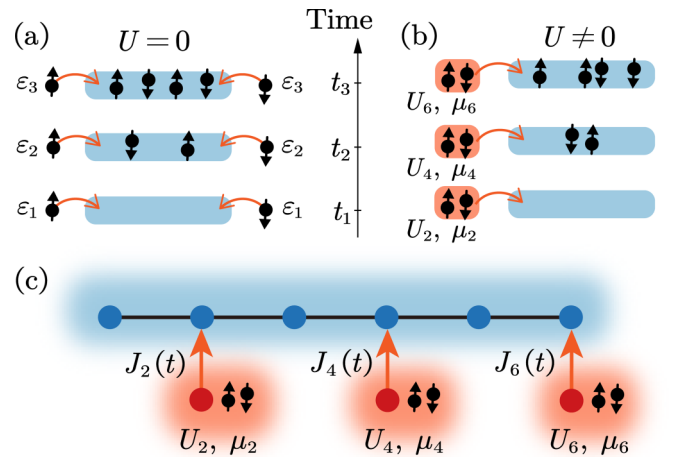


FIG. 4. Schematic of the time-ordered injection process. To reach the ground state of the system, (a) when $U = 0$, the electrons can be injected into the system one by one, without the need of specific order. (b) while for the case of $U \neq 0$, the electrons must be filled into the system pair by pair with order. (c) Configuration of the system and the initial state. The system includes a six-site Hubbard chain and three side-coupled sites with different pair binding energy and chemical potential determined by Eq. (34). The unidirectional coupling J_2 , J_4 , and J_6 (orange arrows) are switched on at ordered times t_1 , t_2 , and t_3 , respectively.

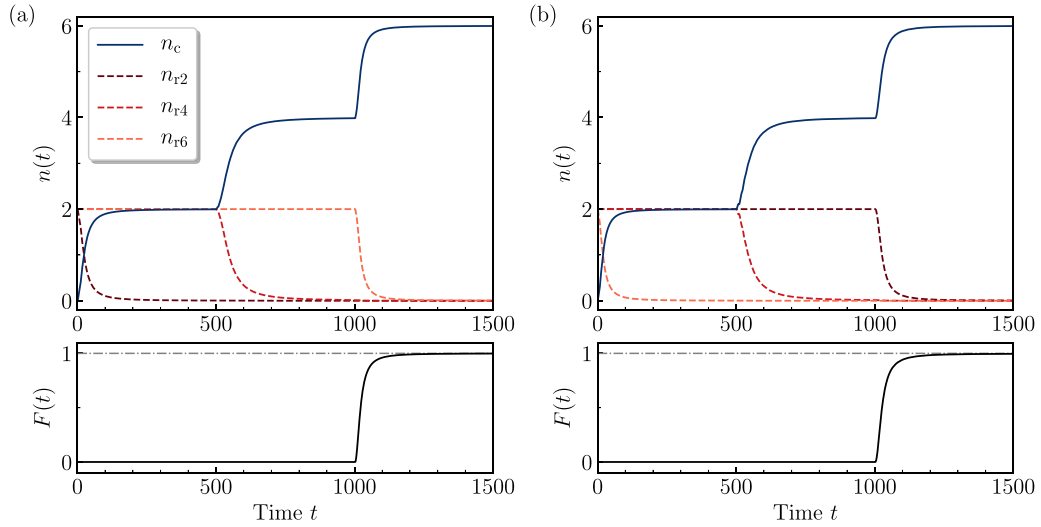


FIG. 5. Numerical results of the particle density and the fidelity for the formation processes of the ground state at half filling. Here n_c [Eq. (39)] and n_{r2l} [Eq. (40)] represent the particle density for the center system and reservoir sites, respectively. The bottom panels show the fidelity $F(t)$ [Eq. (41)] between the evolved state and the target ground state. The system configuration and the initial state are illustrated in Fig. 4(c), where the center system is empty and each side-coupled site has two electron filled. (a) Formation processes of the ground state for system with interaction strength $U = 1$. The time dependent unidirectional coupling $J_{2l}(t)$ is taken as the form in Eq. (35). (b) When $U = 0$, the order in $\{J_{2l}(t)\}$ becomes not necessary. In this case, $J_{2l}(t)$ is taken as another order in Eq. (42). Other parameters of the system: $J_c = 1$, $N = 6$, $J = 0.1$, and $\tau = 501$.

Obviously, H_q is the term for a sequence of quenching with an interval τ .

Based on the above analysis, the dynamics of H_1 is governed by the time evolution operator

$$U(t) = \exp \left[-i \int_0^t H(t') dt' \right]. \quad (36)$$

Initially, the whole system is prepared in the state with H_c being empty while H_r is fully filled, that is

$$|\psi(0)\rangle = \prod_{l=1}^{N/2} d_{2l,\uparrow}^\dagger d_{2l,\downarrow}^\dagger |\text{vac}\rangle. \quad (37)$$

It is expected that the evolved states at $t = n\tau$ satisfy

$$\left. \begin{aligned} |\psi(\tau)\rangle &= |\psi_g(2, 0)\rangle \prod_{l=2}^{N/2} d_{2l,\uparrow}^\dagger d_{2l,\downarrow}^\dagger |\text{vac}\rangle, \\ &\vdots \\ |\psi(n\tau)\rangle &= |\psi_g(2n, 0)\rangle \prod_{l=n+1}^{N/2} d_{2l,\uparrow}^\dagger d_{2l,\downarrow}^\dagger |\text{vac}\rangle, \\ &\vdots \\ |\psi(\infty)\rangle &= |\psi_g(N, 0)\rangle. \end{aligned} \right\} \quad (38)$$

Ideally, it follows that the ground state at half filling is achieved via a sequence of quenching.

It should be noted that the set of parameters $\{\mu_{2l}\}$ obey the order $\mu_2 < \dots < \mu_{2l} < \dots < \mu_N$ and $\{J_{2l}(t)\}$ match this order. When $U = 0$, μ_{2l} reduces to ε_l . Remarkably, the order in $\{J_{2l}(t)\}$ becomes not necessary, i.e., the corresponding ground state can be built by injecting electrons in an arbitrary way [see Figs. 4(a) and 4(b)]. This is a direct reflection of the difference between the ground states of correlated and noninteracting systems.

Numerical simulations for the formation processes of the ground state at half filling are performed for a finite system with $U = 1$ and $U = 0$. We calculate the particle density for

the center system and the reservoir as a function of time, which are defined as

$$n_c = \sum_{l=1}^N \sum_{\sigma=\uparrow,\downarrow} \langle \psi(t) | c_{l,\sigma}^\dagger c_{l,\sigma} | \psi(t) \rangle \quad (39)$$

and

$$n_{r2l} = \sum_{\sigma=\uparrow,\downarrow} \langle \psi(t) | d_{2l,\sigma}^\dagger d_{2l,\sigma} | \psi(t) \rangle, \quad (40)$$

as well as the fidelity between the evolved state and the target ground state

$$F(t) = |\langle \psi(t) | \psi_g(N, 0) \rangle|. \quad (41)$$

Here the target ground state used is obtained by exact diagonalization. In Fig. 5(a), the interaction strength of the system is set as $U = 1$ and the unidirectional coupling $J_{2l}(t)$ is taken as the form in Eq. (35). We can see that the results are in accord with our prediction, while, for the noninteracting case of $U = 0$, we consider the parameter of quenching with

$$J_{2l}(t) = \begin{cases} 0, & t \leq (3-l)\tau, \\ J, & t > (3-l)\tau \end{cases} \quad (42)$$

as an example, which sets a quench in an inverse order. In Fig. 5(b), it is demonstrated that the ground state can be well built, indicating that the order in $\{J_{2l}(t)\}$ becomes not necessary for the noninteracting system. In addition, we note that each binding energy U_{2l} is always negative in the sample we considered. It becomes positive when we consider negative U . The implication of the observation cannot be explained at this stage due to the limitation of the sample size.

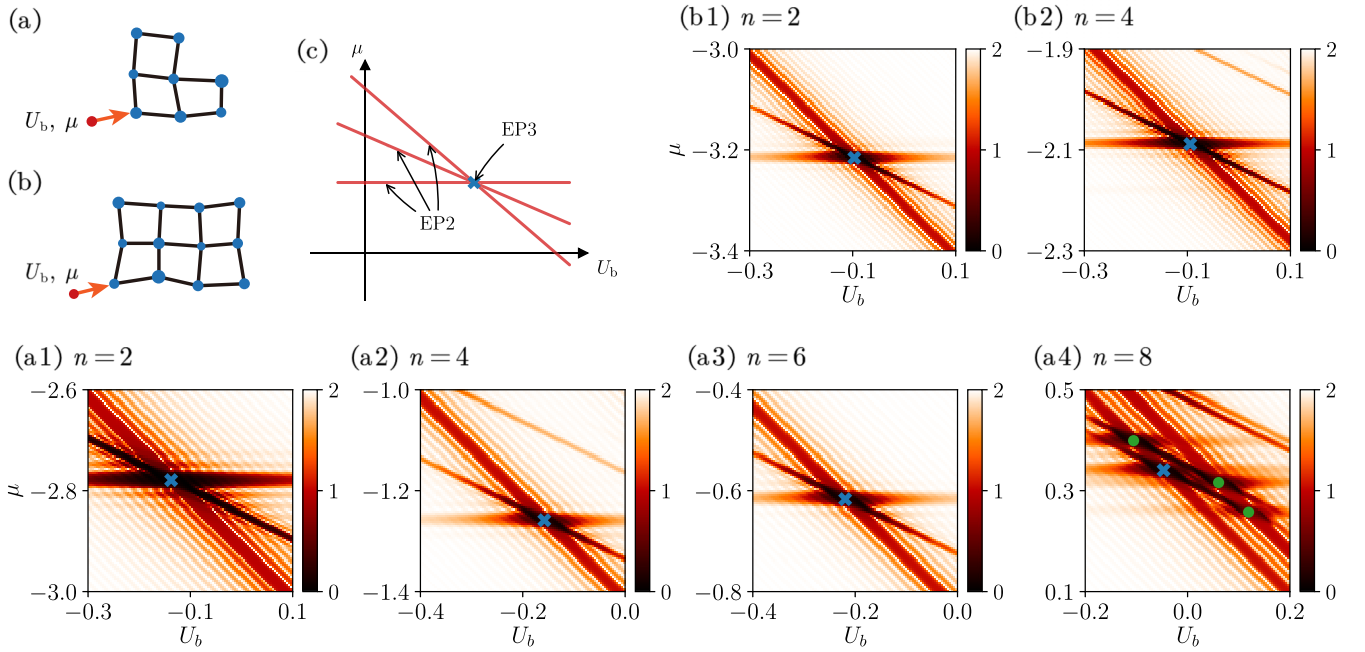


FIG. 6. Panels (a) and (b) are schematics of two 2D lattices. The different lengths of black edges and different sizes of blue solid circles denote the disordered hopping strength $\{J_{l,l'}\}$ and interaction strength $\{U_l\}$. (c) Schematic of the EP2 lines defined in Eqs. (47)–(49), the intersection point (EP3) of which is the resonance condition. Panels (a1)–(a4) and (b1), (b2) are numerical results of the particle density of the side-coupled site for lattices (a) and (b), respectively, with different number of electrons n . For each n , the numerical simulations of time evolution are performed 100×100 times in a uniform 2D mesh of (U_b, μ) . The evolved time of the final states is $t = 300$ for each realization of time evolution. The blue crosses represent values of resonance parameters obtained from exact diagonalization. The green solid circles in (a4) are calculated from the excited states. Other parameters of the system: $N = 8$ and 12 for (a) and (b), and $J_p = 0.05$.

V. DETERMINATIONS OF QUENCHING PARAMETERS AND GROUND STATE

We have demonstrated that the ground state of the Hubbard chain can be built by the quenching under the resonance condition (quenching parameters) in Eq. (34). However, for a more realistic system, these parameters as well as the ground-state energy are actually unknown. A problem arises of how to implement the quenching protocol without the prior knowledge of the Hamiltonian and the quenching parameters. In this section, we show that this problem can be solved by scanning over the parameters of the auxiliary site and observing the number of electrons in it.

Consider the following Hamiltonian:

$$H_2 = H_c + H'_p, \quad (43)$$

with H_c defined in Eq. (2), and the non-Hermitian side-coupled term is

$$H'_p = J_p \sum_{\sigma=\uparrow,\downarrow} c_{\alpha,\sigma}^\dagger c_{p,\sigma} + U_b n_{p,\uparrow} n_{p,\downarrow} + \mu \sum_{\sigma=\uparrow,\downarrow} n_{p,\sigma}. \quad (44)$$

Here α denotes a site of H_c and the parameters $\{J_{l,l'}, U_l\}$ in H_c are assumed to be unknown: in the following numerical calculation, $\{J_{l,l'}\}$ and $\{U_l\}$ are taken as the random samples that are uniformly distributed over the intervals $[1, 1.2)$ and $[0.9, 1.1)$, respectively. The system configurations considered are schematically illustrated in Figs. 6(a) and 6(b).

Similarly with the analysis for the Hermitian system in Sec. II, under the basis defined in Eq. (8), the effective Hamil-

tonian for H_2 can be written as

$$\tilde{h} = \begin{pmatrix} \epsilon_1 & \kappa_1 & \kappa_1 & 0 \\ 0 & \epsilon_2 & 0 & \kappa_2 \\ 0 & 0 & \epsilon_2 & \kappa_2 \\ 0 & 0 & 0 & \epsilon_4 \end{pmatrix}, \quad (45)$$

where the matrix elements

$$\begin{aligned} \epsilon_1 &= E_g(n, 0), \\ \epsilon_2 &= E_g(n-1, 1/2) + \mu, \\ \epsilon_4 &= E_g(n-2, 0) + 2\mu + U_b, \\ \kappa_1 &= \langle 1|H'_p|2 \rangle = \langle 1|H'_p|3 \rangle, \\ \kappa_2 &= \langle 2|H'_p|4 \rangle = \langle 3|H'_p|4 \rangle. \end{aligned} \quad (46)$$

We note that, when varying the parameters (U_b, μ) of the side-coupled site, the matrix \tilde{h} supports three sets of two-state coalescence points (EP2), forming three lines in the parameter space of (U_b, μ) . The equations of three lines respectively have the forms

$$\mu = E_g(n, 0) - E_g(n-1, 1/2), \quad (47)$$

$$U_b + \mu = E_g(n-1, 1/2) - E_g(n-2, 0), \quad (48)$$

$$U_b + 2\mu = E_g(n, 0) - E_g(n-2, 0), \quad (49)$$

wherein the matrix \tilde{h} can be brought into Jordan form that contains a Jordan block of order two by the Jordan decomposition. The intersection point of the three lines is a three-state

TABLE I. (U_b, μ, E_g) obtained from the scanning process and (U'_b, μ', E'_g) obtained from exact diagonalization for lattices (a) and (b) at different number of filled electrons n .

| (a) | Scan | | | Diagonalization | | |
|-----|--------|--------|---------|-----------------|--------|---------|
| | U_b | μ | E_g | U'_b | μ' | E'_g |
| n | | | | | | |
| 2 | -0.167 | -2.770 | -5.706 | -0.138 | -2.779 | -5.696 |
| 4 | -0.133 | -1.267 | -8.373 | -0.157 | -1.259 | -8.371 |
| 6 | -0.194 | -0.626 | -9.819 | -0.220 | -0.617 | -9.824 |
| 8 | -0.018 | 0.330 | -9.177 | -0.047 | 0.341 | -9.190 |
| (b) | Scan | | | Diagonalization | | |
| | U_b | μ | E_g | U'_b | μ' | E'_g |
| n | | | | | | |
| 2 | -0.078 | -3.222 | -6.522 | -0.097 | -3.216 | -6.528 |
| 4 | -0.070 | -2.100 | -10.788 | -0.094 | -2.089 | -10.800 |

coalescence point (EP3), which is also the resonance condition in Eq. (34). The schematic illustration of the three lines of EP2 and point of EP3 is given in Fig. 6(c). We would like to point out that this feature is independent of the dimension and the exact knowledge of parameters $\{J_{l,l'}, U_l\}$ of the Hubbard model.

The above analysis suggests a scanning scheme to determine the quenching parameters and the ground-state energy of the system. As we have shown in the previous section, the system with parameters at EP supports unidirectional dynamics. In the current system, it can be checked that, if the initial state is prepared as $|4\rangle = |\psi_g(n-2, 0)| \uparrow \downarrow \rangle_p$, then after the quench and for a large t , the pair probability at the side-coupled site is dominated by the factors t^{-2} and t^{-4} for parameters (U_b, μ) of EP2 and EP3, respectively. That is, the numbers of electrons at the side-coupled site decay at different rates for parameters of EP2 and EP3. For the case with (U_b, μ) deviating from EPs, the electrons oscillate between the side-coupled site p and the center system H_c . Scanning over (U_b, μ) for a set of realizations of time evolution, the pattern in Fig. 6(c) is expected to be obtained if we observe the evolved-state particle density for the side-coupled site. The initial state $|4\rangle$ with number of electrons n can be built by using the resonance conditions for $n-2$, $n-4$, $n-6$, etc., which are detected from previous scans. Then, using the scanning scheme, the resonance conditions for $n=2, 4, 6, \dots$ can be obtained successively. To verify the performance of the scanning scheme, we conduct numerical simulations with initial state $|\psi(0)\rangle = |\psi_g(n-2, 0)| \uparrow \downarrow \rangle_p$ for different numbers of electrons n , and evolve the state under the Hamiltonian in Eq. (43), with aforementioned disordered parameters $\{J_{l,l'}, U_l\}$. For each n , we scan over the parameters of the side-coupled site (U_b, μ) by 100×100 realizations of time evolution. In practical implementation, one only needs to scan two lines in the parameter space (for instance, two lines with constant μ) to obtain a few points of EP2, and then, connecting them in straight lines, the intersection is the position of the resonance point (EP3). For each realization, the system is reprepared in state $|\psi(0)\rangle$ initially. After a sufficiently long evolved time, we calculate particle density for the side-coupled site. The calculations of time evolution are performed in the truncated subspace of around 100 low-

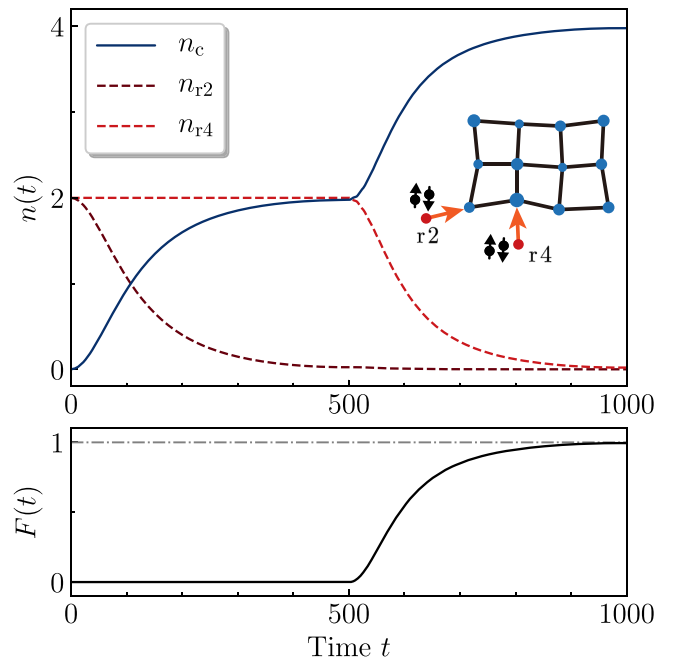


FIG. 7. Numerical results of the particle density and the fidelity for the formation processes of the ground state at filling $n = 4$. Here n_c and n_{r2l} represent the particle density for the center system and reservoir sites, respectively. The inset illustrates the system configuration and the initial state. The bottom panel shows the fidelity $F(t)$ between the evolved state and the target ground state [four-electron ground state $|\psi_g(n=4, s^z=0)\rangle$ obtained from exact diagonalization]. The disordered parameters $\{J_{l,l'}, U_l\}$ are taken to be the same as that of Figs. 6(b1) and 6(b2). The quenching parameters (U_b, μ) with $n=2$ and 4 are taken as the scanning values in Table I(b). Other parameters of the system: $N = 12$, $J_p = 0.05$, and $\tau = 501$.

excited states, since the contribution of the high-excited states are very tiny to the quenching process.

The numerical results are presented in Figs. 6(a1)–6(a4) and 6(b1), 6(b2) for the lattices in Figs. 6(a) and 6(b), respectively. We can clearly see the patterns of EP lines for each n . The blue crosses represent values of resonance parameters obtained from exact diagonalization and Eq. (34), which are well located at the intersection of the EP lines obtained from the scanning numerical simulations. In Fig. 6(a4), more intersection points that come from the low-excited states are obtained. This is verified by the green solid circles that are calculated from Eq. (34) but changing $E_g(n, 0)$ or $E_g(n-1, 1/2)$ to the corresponding first-excited energies. In Table I, we present the scanning values of (U_b, μ) that are obtained from the minimum of the particle density of a side-coupled site in the data of Figs. 6(a1)–6(a4) and 6(b1), 6(b2). Using these scanning values as inputs, the ground-state energy E_g for different n is calculated from Eq. (34). By contrast, E'_g is obtained from exact diagonalization and (U'_b, μ') is calculated from Eq. (34). We can see that, for both lattices, the values of E_g and E'_g are close at each number of filled electron n .

Furthermore, we use the scanning values of quenching parameters (U_b, μ) in Table I(b) to build the four-electron ground states of the 2D lattice in Fig. 6(b). The quenching process is the same as that described in Sec. IV, and the time

evolution here is calculated by the exact diagonalization of the full Hamiltonian in four-particle subspace. With high fidelity between the target ground state $|\psi_g(n=4, s^z=0)\rangle$ and the evolved state at $t=1000$, the numerical results presented in Fig. 7 show the validity of the data obtained from the scanning process, as well as verify that the quenching protocol can be applied to the 2D Hubbard model deviating from half filling.

VI. SUMMARY

In summary, we have proposed a method to build the ground state of a Hubbard model with n electrons to the one with $n+2$ electrons by injecting a bound pair of electrons in the framework of quantum dynamics. The underlying mechanism is the EP dynamics at the resonance. As application, we demonstrated the dynamic formation of the ground state of the Hubbard model at half filling and deviating from half filling. It provides a clear picture for the correlated ground state: it can be obtained by filling a group of bound pair electrons in time order. Each pair with specific filling order has its own binding energy and chemical potential, which can be determined by the proposed scanning scheme. In contrast, when the Hubbard repulsion U is zero, the binding energy vanishes, and then the filling order is not necessary. It is expected that our finding not only provides a method for correlated quantum state engineering, but also reveals the feature of the ground state in an alternative way.

ACKNOWLEDGMENT

This work was supported by National Natural Science Foundation of China (under Grant No. 11874225).

APPENDIX

In this Appendix, we present the derivations on the time evolutions under Hermitian matrix h_R and non-Hermitian matrix \tilde{h}_R to explain the connection and difference between two dynamic processes. For simplicity, we omit the diagonal elements $E_g(n, 0)$ in both cases.

(i) The eigenvectors and eigenvalues of matrix

$$h_R = \begin{pmatrix} 0 & \kappa_1 & \kappa_1 & 0 \\ \kappa_1 & 0 & 0 & \kappa_2 \\ \kappa_1 & 0 & 0 & \kappa_2 \\ 0 & \kappa_2 & \kappa_2 & 0 \end{pmatrix} \quad (A1)$$

are in the form

$$|\phi_0\rangle = \frac{\sqrt{2}}{\varepsilon} \begin{pmatrix} -\kappa_2 \\ 0 \\ 0 \\ \kappa_1 \end{pmatrix}, \quad E_0 = 0,$$

$$|\phi_{\pm}\rangle = \frac{1}{\varepsilon} \begin{pmatrix} 2\kappa_1 \\ \pm\varepsilon \\ \pm\varepsilon \\ 2\kappa_2 \end{pmatrix}, \quad E_{\pm} = \pm\varepsilon,$$

$$|\phi_1\rangle = \begin{pmatrix} 0 \\ -1 \\ 1 \\ 0 \end{pmatrix}, \quad E_1 = 0, \quad (A2)$$

where $\varepsilon = \sqrt{2(\kappa_1^2 + \kappa_2^2)}$. Straightforward derivation shows that

$$|1\rangle = \frac{\kappa_1\varepsilon(|\phi_+\rangle + |\phi_-\rangle) - 2\sqrt{2}\kappa_2\varepsilon|\phi_0\rangle}{4(\kappa_1^2 + \kappa_2^2)} \quad (A3)$$

and

$$e^{-i\tilde{h}_R t}|1\rangle = \frac{1}{2(\kappa_1^2 + \kappa_2^2)} \begin{pmatrix} 2\kappa_1^2 \cos(\varepsilon t) + 2\kappa_2^2 \\ -i\varepsilon\kappa_1 \sin(\varepsilon t) \\ -i\varepsilon\kappa_1 \sin(\varepsilon t) \\ 2\kappa_2\kappa_1 \cos(\varepsilon t) - 2\kappa_2\kappa_1 \end{pmatrix}. \quad (A4)$$

Then the pair probability at the side-coupled site is

$$|\langle 4|e^{-i\tilde{h}_R t}|1\rangle|^2 = \frac{4(\kappa_2\kappa_1)^2 \cos^2(\varepsilon t/2)}{(\kappa_1^2 + \kappa_2^2)^2}, \quad (A5)$$

with the maximum

$$\max|\langle 4|e^{-i\tilde{h}_R t}|1\rangle|^2 = \frac{4(\kappa_2\kappa_1)^2}{(\kappa_1^2 + \kappa_2^2)^2}. \quad (A6)$$

It approaches to unit when $\kappa_1 = \kappa_2$.

(ii) For the non-Hermitian matrix

$$\tilde{h}_R = \begin{pmatrix} 0 & 0 & 0 & 0 \\ \kappa_1 & 0 & 0 & 0 \\ \kappa_1 & 0 & 0 & 0 \\ 0 & \kappa_2 & \kappa_2 & 0 \end{pmatrix}, \quad (A7)$$

we simply have

$$(\tilde{h}_R)^2 = \begin{pmatrix} 0 & 0 & 0 & 0 \\ 0 & 0 & 0 & 0 \\ 0 & 0 & 0 & 0 \\ 2\kappa_1\kappa_2 & 0 & 0 & 0 \end{pmatrix} \quad (A8)$$

and

$$(\tilde{h}_R)^3 = \mathbf{0}. \quad (A9)$$

Then we have

$$e^{-i\tilde{h}_R t} = \begin{pmatrix} 1 & 0 & 0 & 0 \\ -it\kappa_1 & 1 & 0 & 0 \\ -it\kappa_1 & 0 & 1 & 0 \\ -t^2\kappa_1\kappa_2 & -it\kappa_2 & -it\kappa_2 & 1 \end{pmatrix}, \quad (A10)$$

which results in

$$e^{-i\tilde{h}_R t}|1\rangle = \begin{pmatrix} 1 \\ -it\kappa_1 \\ -it\kappa_1 \\ -t^2\kappa_1\kappa_2 \end{pmatrix}. \quad (A11)$$

It turns out that

$$e^{-i\tilde{h}_R t}|1\rangle \rightarrow |4\rangle \quad (A12)$$

for a sufficiently long time without the need of $\kappa_1 = \kappa_2$.

- [1] J. Hubbard, Electron correlations in narrow energy bands, *Proc. R. Soc. A* **276**, 238 (1963).
- [2] M. Imada, A. Fujimori, and Y. Tokura, Metal-insulator transitions, *Rev. Mod. Phys.* **70**, 1039 (1998).
- [3] R. Staudt, M. Dzierzawa, and A. Muramatsu, Phase diagram of the three-dimensional Hubbard model at half filling, *Eur. Phys. J. B* **17**, 411 (2000).
- [4] P. W. Anderson, The resonating valence bond state in La_2CuO_4 and superconductivity, *Science* **235**, 1196 (1987).
- [5] P. Lee, N. Nagaosa, and X.-G. Wen, Doping a Mott insulator: Physics of high-temperature superconductivity, *Rev. Mod. Phys.* **78**, 17 (2006).
- [6] M. F. Parsons, A. Mazurenko, C. S. Chiu, G. Ji, D. Greif, and M. Greiner, Site-resolved measurement of the spin-correlation function in the Fermi-Hubbard model, *Science* **353**, 1253 (2016).
- [7] R. Bistritzer and A. H. MacDonald, Moiré bands in twisted double layer graphene, *Proc. Natl. Acad. Sci. USA* **108**, 12233 (2011).
- [8] Y. Cao, J. Y. Luo, V. Fatemi, S. Fang, J. D. Sanchez-Yamagishi, K. Watanabe, T. Taniguchi, E. Kaxiras, and P. Jarillo-Herrero, Superlattice-Induced Insulating States and Valley-Protected Orbits in Twisted Bilayer Graphene, *Phys. Rev. Lett.* **117**, 116804 (2016).
- [9] K. Kim, A. DaSilva, S. Huang, B. Fallahzad, S. Larentis, T. Taniguchi, K. Watanabe, B. J. LeRoy, A. H. MacDonald, and E. Tutuc, Tunable moiré bands and strong correlations in small twist angle bilayer graphene, *Proc. Natl. Acad. Sci. USA* **114**, 3364 (2017).
- [10] Y. Cao, V. Fatemi, A. Demir, S. Fang, S. L. Tomarken, J. Y. Luo, J. D. Sanchez-Yamagishi, K. Watanabe, T. Taniguchi, E. Kaxiras, R. C. Ashoori, and P. Jarillo-Herrero, Correlated insulator behaviour at half-filling in magic-angle graphene superlattices, *Nature (London)* **556**, 80 (2018).
- [11] Y. Cao, V. Fatemi, S. Fang, K. Watanabe, T. Taniguchi, E. Kaxiras, and P. Jarillo-Herrero, Unconventional superconductivity in magic-angle graphene superlattices, *Nature (London)* **556**, 43 (2018).
- [12] M. Yankowitz, S. Chen, H. Polshyn, Y. Zhang, K. Watanabe, T. Taniguchi, D. Graf, A. F. Young, and C. R. Dean, Tuning superconductivity in twisted bilayer graphene, *Science* **363**, 1059 (2019).
- [13] X. Lu, P. Stepanov, W. Yang, M. Xie, M. A. Aamir, I. Das, C. Urgell, K. Watanabe, T. Taniguchi, G. Zhang, A. Bachtold, A. H. MacDonald, and D. K. Efetov, Superconductors, orbital magnets and correlated states in magic-angle bilayer graphene, *Nature (London)* **574**, 653 (2019).
- [14] P. Calabrese and J. Cardy, Time Dependence of Correlation Functions Following a Quantum Quench, *Phys. Rev. Lett.* **96**, 136801 (2006).
- [15] S. R. Manmana, S. Wessel, R. M. Noack, and A. Muramatsu, Strongly Correlated Fermions after a Quantum Quench, *Phys. Rev. Lett.* **98**, 210405 (2007).
- [16] A. Iucci and M. A. Cazalilla, Quantum quench dynamics of the Luttinger model, *Phys. Rev. A* **80**, 063619 (2009).
- [17] M. Schiró and M. Fabrizio, Quantum quenches in the Hubbard model: Time-dependent mean-field theory and the role of quantum fluctuations, *Phys. Rev. B* **83**, 165105 (2011).
- [18] M. Moeckel and S. Kehrein, Interaction Quench in the Hubbard Model, *Phys. Rev. Lett.* **100**, 175702 (2008).
- [19] M. Eckstein, M. Kollar, and P. Werner, Thermalization after an Interaction Quench in the Hubbard Model, *Phys. Rev. Lett.* **103**, 056403 (2009).
- [20] C. Kollath, A. M. Läuchli, and E. Altman, Quench Dynamics and Nonequilibrium Phase Diagram of the Bose-Hubbard Model, *Phys. Rev. Lett.* **98**, 180601 (2007).
- [21] G. Biroli, C. Kollath, and A. M. Läuchli, Effect of Rare Fluctuations on the Thermalization of Isolated Quantum Systems, *Phys. Rev. Lett.* **105**, 250401 (2010).
- [22] M. Greiner, O. Mandel, T. W. Hänsch, and I. Bloch, Collapse and revival of the matter wave field of a Bose-Einstein condensate, *Nature (London)* **419**, 51 (2002).
- [23] T. Kinoshita, T. Wenger, and D. S. Weiss, A quantum Newton's cradle, *Nature (London)* **440**, 900 (2006).
- [24] S. Trotzky, Y.-A. Chen, A. Flesch, I. P. McCulloch, U. Schollwöck, J. Eisert, and I. Bloch, Probing the relaxation towards equilibrium in an isolated strongly correlated one-dimensional Bose gas, *Nat. Phys.* **8**, 325 (2012).
- [25] M. Cheneau, P. Barmettler, D. Poletti, M. Endres, P. Schauß, T. Fukuhara, C. Gross, I. Bloch, C. Kollath, and S. Kuhr, Light-cone-like spreading of correlations in a quantum many-body system, *Nature (London)* **481**, 484 (2012).
- [26] M. Gring, M. Kuhnert, T. Langen, T. Kitagawa, B. Rauer, M. Schreitl, I. Mazets, D. Adu Smith, E. Demler, and J. Schmiedmayer, Relaxation and prethermalization in an isolated quantum system, *Science* **337**, 1318 (2012).
- [27] N. Syassen, D. M. Bauer, M. Lettner, T. Volz, D. Dietze, J. J. García-Ripoll, J. I. Cirac, G. Rempe, and S. Dürr, Strong dissipation inhibits losses and induces correlations in cold molecular gases, *Science* **320**, 1329 (2008).
- [28] W. S. Bakr, J. I. Gillen, A. Peng, S. Fölling, and M. Greiner, A quantum gas microscope for detecting single atoms in a Hubbard-regime optical lattice, *Nature (London)* **462**, 74 (2009).
- [29] B. Zhu, B. Gadway, M. Foss-Feig, J. Schachenmayer, M. L. Wall, K. R. A. Hazzard, B. Yan, S. A. Moses, J. P. Covey, D. S. Jin, J. Ye, M. Holland, and A. M. Rey, Suppressing the Loss of Ultracold Molecules via the Continuous Quantum Zeno Effect, *Phys. Rev. Lett.* **112**, 070404 (2014).
- [30] M. F. Parsons, F. Huber, A. Mazurenko, C. S. Chiu, W. Setiawan, K. Wooley-Brown, S. Blatt, and M. Greiner, Site-Resolved Imaging of Fermionic ${}^6\text{Li}$ in an Optical Lattice, *Phys. Rev. Lett.* **114**, 213002 (2015).
- [31] L. W. Cheuk, M. A. Nichols, M. Okan, T. Gersdorf, V. V. Ramasesh, W. S. Bakr, T. Lompe, and M. W. Zwierlein, Quantum-Gas Microscope for Fermionic Atoms, *Phys. Rev. Lett.* **114**, 193001 (2015).
- [32] L. W. Cheuk, M. A. Nichols, K. R. Lawrence, M. Okan, H. Zhang, and M. W. Zwierlein, Observation of 2D Fermionic Mott Insulators of ${}^{40}\text{K}$ with Single-Site Resolution, *Phys. Rev. Lett.* **116**, 235301 (2016).
- [33] T. Tomita, S. Nakajima, I. Danshita, Y. Takasu, and Y. Takahashi, Observation of the Mott insulator to superfluid crossover of a driven-dissipative Bose-Hubbard system, *Sci. Adv.* **3**, e1701513 (2017).
- [34] K. Sponselee, L. Freystatzky, B. Abeln, M. Diem, B. Hundt, A. Kochanek, T. Ponath, B. Santra, L. Mathey, K. Sengstock, and C. Becker, Dynamics of ultracold quantum gases in the dissipative Fermi-Hubbard model, *Quantum Sci. Technol.* **4**, 014002 (2018).

- [35] S. A. Sato, P. Tang, M. A. Sentef, U. D. Giovannini, H. Hübener, and A. Rubio, Light-induced anomalous Hall effect in massless Dirac fermion systems and topological insulators with dissipation, *New J. Phys.* **21**, 093005 (2019).
- [36] T. Esslinger, Fermi-Hubbard physics with atoms in an optical lattice, *Annu. Rev. Condens. Matter Phys.* **1**, 129 (2020).
- [37] C. Booker, B. Buča, and D. Jaksch, Non-stationarity and dissipative time crystals: Spectral properties and finite-size effects, *New J. Phys.* **22**, 085007 (2020).
- [38] X. Z. Zhang, L. Jin, and Z. Song, Dynamic magnetization in non-Hermitian quantum spin systems, *Phys. Rev. B* **101**, 224301 (2020).
- [39] C. M. Bender and S. Boettcher, Real Spectra in Non-Hermitian Hamiltonians Having PT Symmetry, *Phys. Rev. Lett.* **80**, 5243 (1998).
- [40] A. Mostafazadeh, Pseudo-Hermiticity versus PT symmetry: The necessary condition for the reality of the spectrum of a non-Hermitian Hamiltonian, *J. Math. Phys.* **43**, 205 (2002).
- [41] L. Jin and Z. Song, Physics counterpart of the PT non-Hermitian tight-binding chain, *Phys. Rev. A* **81**, 032109 (2010).
- [42] M. Müller and I. Rotter, Exceptional points in open quantum systems, *J. Phys. A: Math. Theor.* **41**, 244018 (2008).
- [43] W. D. Heiss, The physics of exceptional points, *J. Phys. A: Math. Theor.* **45**, 444016 (2012).
- [44] I. Rotter and J. P. Bird, A review of progress in the physics of open quantum systems: Theory and experiment, *Rep. Prog. Phys.* **78**, 114001 (2015).
- [45] E. H. Lieb, Two Theorems on the Hubbard Model, *Phys. Rev. Lett.* **62**, 1201 (1989).